Journal of Hydroinformatics

Journal of Hydroinformatics Vol 26 No 1, 304 doi: 10.2166/hydro.2023.427

Experimental and numerical investigation of Engineered Injection and Extraction (EIE) induced with three-dimensional flow field

Farsana M. Asha[a,b,*], N. Sajikumar[a,c] and E. A. Subaida[a]

[a] Department of Civil Engineering, Government Engineering College, Thrissur, Kerala, India
[b] A. P. J. Abdul Kalam Technological University, Thiruvananthapuram, Kerala, India
[c] Principal Consultant, WRPM Consultants, Thrissur, India
*Corresponding author. E-mail: ashafarsana@gectcr.ac.in

ABSTRACT

In situ groundwater remediation technique is a commonly adopted method for the treatment of contaminated groundwater and the porous media associated with it. Engineered Injection and Extraction (EIE) has evolved as an improved methodology for in situ remediation, where sequential injection and extraction of clean water around the treatment area enhances the spreading of treatment reagents by inducing additional flow fields. Conventional EIE studies were based on flow fields in two dimensions. There are only limited experimental and theoretical studies exploring the potential of inducing a three-dimensional flow field using EIE. The present study experimentally and numerically evaluates the effect of a three-dimensional flow field induced by partially screened wells. EIE experiments were conducted on a laboratory-scale aquifer model with laterite soil as the porous medium. Tracer transport in porous medium was studied by measuring the concentration at various observation points and enhanced dilution was observed when EIE was employed with partially screened wells. Experimental observations were also used to calibrate and validate the numerical model developed using Visual MODFLOW Flex. Enhancement in spreading was quantified in terms of concentration mass attenuation and maximum mass attenuation was observed when EIE was employed with partially screened wells.

Key words: conservative tracer transport, dispersivity, Engineered Injection and Extraction (EIE), experimental validation, modelling aquifer

HIGHLIGHTS

- Experimental investigation of engineered injection extraction (EIE) in three-dimension is carried out in this study using a laboratory-scale aquifer model.
- Study experimentally proved the improvement in spreading when EIE is employed with partially screened wells over EIE with fully screened wells.
- Calibrated and validated numerical model created using Visual MODFLOW Flex using experimental observations.

1. INTRODUCTION

Remediation of groundwater contamination is a major concern for water professionals from all over the world. Various technologies have been developed for remediating contaminated groundwater. Contaminated groundwater often defiles the porous media matrix in contact with it and vice versa. Hence, remediation of a contaminated aquifer should always address the treatment for both water and porous media matrix. In situ groundwater remediation techniques have gained much recognition in this context. It works by injecting a suitable reagent into the contaminated aquifer, thus remediating groundwater and the porous media matrix simultaneously. It is more convenient compared to ex situ technologies such as pump and treat where contaminated water is extracted, treated offsite and injected back. But, in most of the in situ treatment methods, the remediation remains incomplete owing to the laminar nature of groundwater flow causing a lack of intermixing between the treatment reagent and the contaminant (Zhang *et al.* 2009). The extent of spreading of reagent into the aquifer is a crucial factor in deciding the efficacy of any in situ remediation technique.

Studies on the spreading of reagents (for remediation) in aquifers are mainly of two broad categories. First is passive spreading which takes place as a result of inherent properties of the aquifer and natural flow field and the second is active spreading which takes place as a result of deliberately induced flow fields within the aquifer (Kapoor & Kitanidis 1996). Several

numerical models that dealt with active spreading in porous media have been reported in the literature. Pulsed dipole by Jones & Aref (1988) was one among them. Stremler *et al.* (2004) experimented with the pulsed dipole model to create enhanced spreading in porous media, which was later applied for groundwater remediation by Sposito (2006). Similar approaches to pulsed dipole were oscillating well triplets by Bagtzoglou & Oates (2007) and rotated potential mixing (RPM) protocol by Trefry *et al.* (2012). All these methods were found to increase spreading in porous media in response to the unsteady flow fields created by using different active pumping protocols. A pulsed dipole has limitations when applied to real aquifers as complete mixing is difficult to achieve without proper reinjection rules (Radabaugh *et al.* 2009; Mays & Neupauer 2012). This method also causes clogging in pumps arising from the extraction of reagents and contaminants simultaneously (Li *et al.* 2009). Engineered Injection and Extraction (EIE) was introduced by Mays & Neupauer (2012), which overcomes the above-mentioned drawbacks.

EIE is an advanced in situ remediation technique in which a suitable treatment reagent is introduced into a contaminated aquifer and a series of injections and extraction of clean water is performed in an arrangement of surrounding wells that can generate chaotic advection(depending on the resulting velocity field). Chaotic advection creates velocity variations and complex particle trajectories in laminar flows (Ottino 1990). EIE is said to stretch and fold the reagent and contaminant plume thereby increasing mixing and thus improving contaminant degradation. Chaotic advection provides a theoretical framework for the stretching and folding of the treatment reagent and the contaminant plume in aquifers during EIE (Mays & Neupauer 2012). Several numerical investigations on enhanced spreading by chaotic advection generated in response to EIE have been found in the literature (Mays & Neupauer 2010, 2012; Piscopo *et al.* 2011, 2013; Neupauer & Mays 2015; Piscopo *et al.* 2015; Greene *et al.* 2017). The numerical investigations showed the potential of EIE in the enhancement of spreading and reaction under various scenarios.

Most of the studies related to EIE and chaotic advection dealt with two-dimensional analysis. Very few attempts have been made to develop EIE in three dimensions. Trefry *et al.* (2012), suggested developing a spherical equivalent of the active spreading protocol for inducing a truly three-dimensional spreading in aquifers. Asha *et al.* (2021) attempted the possibility of enhancing three-dimensional spreading by emplacement of partially screened wells in EIE. They used a three-dimensional homogeneous and confined aquifer model domain and simulated the behaviour of particle movement under EIE with partially screened wells. Enhancement in spreading was observed when EIE was attempted with partially screened wells. However, most of the numerical models describing EIE lack proper experimental validation. Conducting experiments to predict the transport processes in porous media and visualising the process is always a topic of utmost importance. A few experimental studies related to chaotic advection in porous media have been reported (Zhang *et al.* 2009; Nissan *et al.* 2017; Roth 2018; Cho *et al.* 2019). Zhang *et al.* (2009) conducted an experiment in a sand-packed flow cell using the oscillating well triplet reported by Bagtzoglou & Oates (2007). Nissan *et al.* (2017) conducted a tracer transport experiment for an unsteady flow through a column packed with sand and showed an increase in the spreading under such flow conditions. Roth (2018) conducted an experimental investigation of scalar spreading as a result of EIE in a homogeneous porous media by using a two-dimensional flow apparatus and showed that EIE could lead to enhanced spreading. A field-scale study of chaotic advection was reported by Cho *et al.* (2019) in which they employed an active pumping protocol (RPM) and studied the enhancement in plume spreading in an experimental lock gate created in a sand pit area. They employed fully screened wells for active pumping and hence, the active flow essentially remained two-dimensional in nature.

Large-scale field experiments provide a clear insight into the actual process, but managing and controlling various unforeseen processes is troublesome. Field tests also involve time-consuming procedures and are expensive; making them difficult to execute. Laboratory experiments are comparatively easier and give better control of the experimental conditions. Considering the ambiguity associated with porous media characteristics (such as conductivity, dispersivity, and porosity), every numerical model needs to be experimentally validated to get much refined and reliable numerical results. EIE in three dimensions employing partially screened wells was numerically simulated by Asha *et al.* (2021), and enhanced spreading in terms of particle trajectories was presented. The study showed enhanced spreading through flow modelling and did not include transport modelling. To get a complete insight into spreading in three dimensions by employing partially screened wells in EIE, the transport of the contaminant should also be considered. The findings based on transport should be experimentally validated before further investigations for optimising the spreading in three dimensions. Therefore, the current study aims to assess the efficacy of EIE in enhancing the three-dimensional spreading of a conservative tracer in laterite soil media, in response to a three-dimensional flow field (created by employing partially screened wells), through numerical simulation and experimental

validation. To the best of our knowledge, this is the first attempt at experimental investigation of EIE (with partially screened wells) in three dimensions using natural porous media.

2. MATERIALS AND METHODOLOGY

2.1. Characterisation of soil sample

Laterite soil sample that passed through a 6 mm IS sieve was taken for the study. The soil was weighed and filled in layers with a fixed height of fall and lightly compacted equally in each layer to ensure uniform packing density. After filling, the soil was saturated by filling water in the outer water chambers and allowing ample time for saturation. The soil samples were tested for various transport and flow parameters prior to the experiment.

The permeability, porosity, grain size analysis, and dispersivity of the laterite soil sample were experimentally estimated. The permeability of the soil sample was determined by using the constant head permeability test (IS 2720 part 17). The soil sample was filled in the permeameter with the same density as that was filled in the experimental glass tank. The average permeability value was observed as 3.5×10^{-5} m/s. The porosity of the soil sample with the same density as that of the model was determined by using saturation of soil as described in the index properties determination by Matko (2003). The porosity of the soil was observed as 0.36. The particle size distribution of the sample was also determined by using sieve analysis and the particle size distribution chart was utilised during the design of the well screen in Section 2.2.

2.1.1. Dispersivity

The value of dispersivity plays a major role in controlling plume migration. Dispersivity can be defined as the ratio of dispersion coefficient and flow velocity in the absence of diffusion (Bear 1972). Longitudinal dispersivity was empirically determined in this study by using a classic column experiment representing one-dimensional form of the advection-dispersion equation (Freeze & Cherry 1979) given by:

$$\frac{\partial C}{\partial t} = D_x \frac{\partial^2 C}{\partial x^2} - v_x \frac{\partial C}{\partial x} \tag{1}$$

where v_x and C are the average linear groundwater velocity and concentration of the contaminant, respectively. The term D_x is the coefficient of hydrodynamic dispersion in the longitudinal direction given by:

$$D_x = (\alpha_x \times V) + D^* \tag{2}$$

where α_x (m) is the dispersivity (longitudinal), V (m/s) is the pore water velocity, and D^* is the molecular diffusion (m^2/s)

For the column experiment, the tracer solution was continuously introduced into a column filled with soil samples in the same density as filled in the glass tank. The breakthrough curve for the NaCl tracer was plotted and was fitted with a solution of one-dimensional advection-dispersion Equation (1) by Ogata (1970) to evaluate the dispersivity of soil. The breakthrough curve is shown in Supplementary material Appendix (Figure A1). The dispersivity was determined by following the method mentioned in Chapter 9, Freeze & Cherry (1979) and the value was obtained as 0.115 m. The range of dispersivity varies with different factors such as the length of the soil column, saturation, soil texture and flow velocity (Zhuang *et al.* 2021). Huang *et al.* (1996)) observed that the values of the dispersivity for the homogeneous sandy column ranged from 0.001 to 0.3 m, while those for heterogeneous columns were as high as 2 m. The empirically determined value of longitudinal dispersivity lies within the above-mentioned ranges. This value was assigned as the longitudinal dispersivity for the initial numerical simulation. During the calibration of the numerical model, the ratio of horizontal to vertical dispersivity was changed in a trial and error method to fix the final ratio.

2.2. Experimental setup

The aquifer model was set up in a tank made of toughened glass with a mild steel frame with outer dimensions 1.3 m × 1 m × 1 m as shown in Figure 1. The glass tank was subdivided into three chambers by using perforated multi-wood panels to allow flow from the outer chambers to the middle chamber. Perforated panels were kept at a distance of 15 cm from either side of the tank and affixed with the help of a mild steel frame and acrylic glue to avoid bulging. The laterite soil sample was filled in the middle chamber. The perforated panels were covered with fine plastic meshes on the inner sides to avoid the escape of fine soil into the outer chamber. The arrangement of two water chambers on either side of the soil chamber was meant to

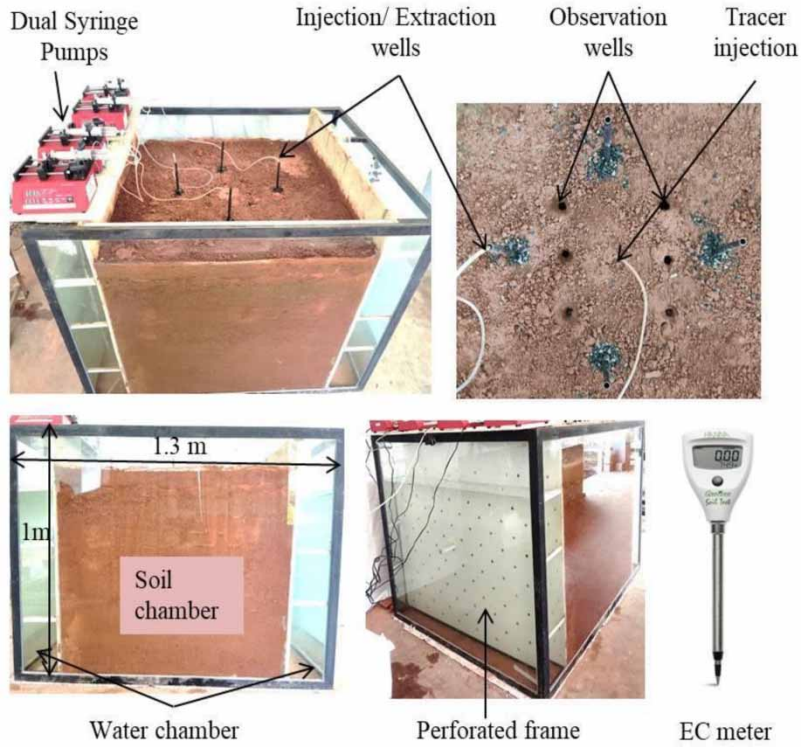

Figure 1 | Experimental setup in different views with its components.

create flow in a particular direction, though not used in the present study. Other components include dual syringe pumps and plumbing kit for injection and extraction of fluids, and a soil electrical conductivity (EC) meter for measuring concentration at observation points (Figure 1).

To represent injection/extraction wells, perforated carbon fibre tubes of 8 mm inner diameter of 1 m length were placed at the required position. Perforations were designed based on the guidelines provided by Raghunath (2007). The grain size distribution of formation was considered while deciding the size of perforations such that the size of perforations lay between D40 and D70 of aquifer material. Four holes of 2.5 mm diameter were drilled along the circumference of the tube and these holes were provided at a distance of 8 mm c/c along the length. A gravel pack is required if the aquifer material is homogeneous with uniformity coefficient $\mathrm{Cu} < 3$ or effective size $D_{10} < 0.25$ mm. Gravel packing was not necessary as the experimentally observed values of uniformity coefficient and effective size of particles were 7.75 and 0.29 mm, respectively. However, a small thickness of gravel was packed around the perforated tubes to avoid extraction of very fine soil particles that are likely to clog the valves of syringe pumps. The gravel size was designed such that D_{30} of gravel pack lay between four to six times D_{30} of particles of the soil (Raghunath 2007).

2.2.1. Injection and extraction procedure

In the present study, programmable dual syringe pumps were used for tracer injection and for performing EIE (Figure 1). The procedure for carrying out the experiment is detailed below. One set of dual-pump systems comprises two syringe pumps (Dual NE 4000-New Era Syringe pumps) connected together by using a CBL dual-3 cable creating an automated continuous operation of the pumping system. The syringe diameter is 26.59 mm which can hold up to 60 ml of fluid. The volume and rate of fluid to be injected/extracted by the pump can be assigned prior to the experiment. Two pumps work together in dual mode for continuous injection and extraction with the help of a dual-pump plumbing kit. The dual-pump plumbing kit consists of check valves through which the syringes are connected to injection/extraction tubes. Injection happens through one valve and extraction happens through the other. Once the pumps are configured to work in dual mode, one pump works as the master controller (represented as 'M' in Figure 2) and the other as the secondary pump ('S' in Figure 2). When the master pump is programmed with a continuous infusion programme, the secondary pump will always pump in the opposite

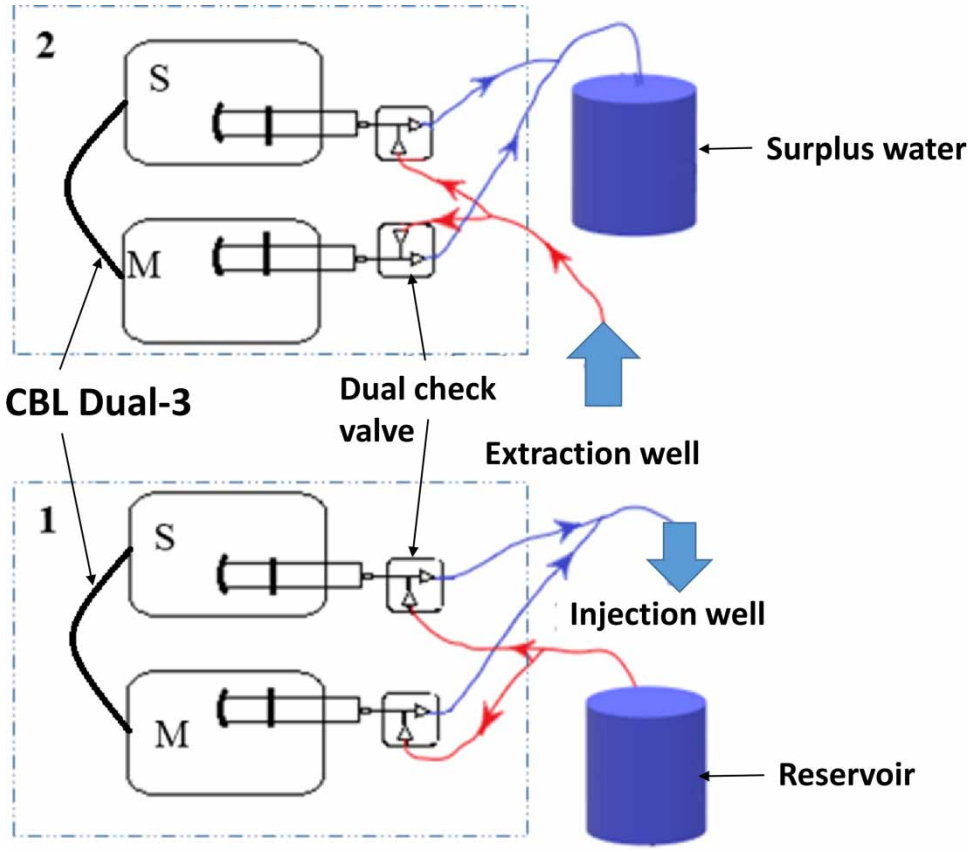

Figure 2 | Schematic representation of active pumping protocol with dual syringe pumps.

direction. A proper plumbing system along with a dual check valve, will create a continuous injection/extraction system. Figure 2 shows the schematic representation of the major components and the pumping schemes for injection into wells and extraction from wells. Scheme 1 in Figure 2 represents extraction from a reservoir and injection into a well (injection phase). Scheme 2 in Figure 2 represents extraction from wells and injection into surplus reservoirs (extraction phase).

For a passive experiment, one set of dual syringe pumps is used. Each syringe is connected to a dual check valve as shown in Figure 2 and they work together in dual mode to continuously inject the tracer at the given pumping rate. The injection tube is buried into the soil such that the tip of the tube is at the required depth (mid-depth). During one cycle, the master pump (M) injects the tracer solution into the injection well and simultaneously the secondary pump (S) withdraws the tracer solution from the reservoir as shown in scheme 1 in Figure 2. Once the master pump finishes injecting the volume assigned, the next cycle starts and the process gets reversed. i.e, the Master pump extracts solution from the reservoir and the secondary pump injects the tracer into an injection well. In either way, it is ensured that continuous tracer injection takes place at the injection well. The rate and volume of fluid for injection/extraction will be preset on the master pump.

During the active experiment, both the schemes 1 and 2 are used alternatively. For the first 15 min, the tracer injection will be carried out in the same manner as in the passive case. Once the tracer injection period stops, the active pumping protocol starts as per the pumping schedule shown in Figure 3. The pumping schedule was adapted from Mays & Neupauer (2012) and scaled according to domain size.

Positive values in the graph (Figure 3) represent injection and negative values represent extraction. As per the pumping schedule, the first two steps are injection at the east and west wells. For this, the injection tube of one set of dual syringe pumps is carefully immersed into the west well up to mid-depth and injection according to the rate specified in the graph is performed. Meanwhile, the injection tube of the other set of dual pumps is kept immersed into the east well to start injection immediately after the injection at the west well stops. The same procedure is repeated for extraction using scheme 2. Only one set of dual syringe pumps operates at a time. Hence, the other set of pumps can be set for the

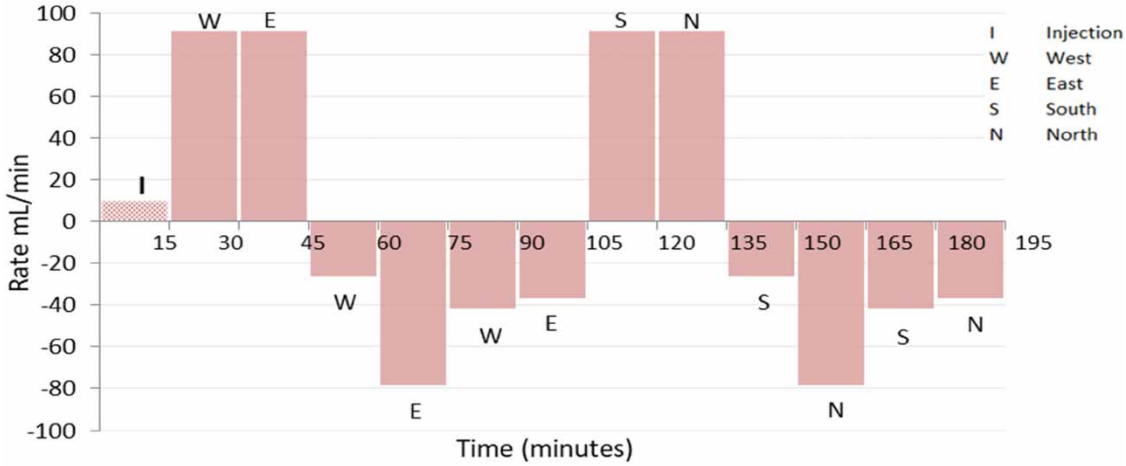

Figure 3 | Pumping schedule (W, E, S, and N represents the wells in that direction w.r.t. injection well (I)).

upcoming withdrawal or pumping at the given rate according to the pumping schedule. The injection and extraction tubes are interchanged and immersed into the required wells as per the schedule. The extracted water from wells is stored in a surplus reservoir rather than a freshwater reservoir to monitor the concentration and make sure that no tracer solution is getting extracted.

2.2.2. Concentration observation procedure

Three sets of experiments were conducted in the experimental setup: one passive experiment and two active experiments. All the experiments were conducted for 195 min and the tracer concentrations were measured at observation points. The conservative tracer used in this study was NaCl. The concentration of NaCl can be measured in terms of EC as it forms an electrolyte solution when dissolved in water. The EC of the solution is directly proportional to the $Na+$ and Cl^- ions present in the water and thus represents the concentration of NaCl. Soil EC-meter (Groline, HI98331 Soil Test) as shown in Figure 1 was used in this study to measure EC of samples. It measures ionic concentration in soil and water in terms of EC. It contains a stainless steel penetration electrode which measures EC in the range 0.00–4.00 mS/cm. EC-meter was calibrated and a concentration vs. conductivity chart was created.

Six observation wells were selected for measuring tracer concentrations at different times. Samples were taken from two layers for the passive experiment and from three layers for the active experiment. The sampling points for passive and active experiments are shown in Appendix (Supplementary material, Figure A2). Samples were taken from different vertical levels using a thin suction rod and were measured for EC values. The time and EC values were recorded manually for each observation point. The observation values obtained were in mS/cm which was converted into mg/l with the help of calibration charts. Observations taken at different intervals were stored as observed concentration time series well data for calibration and validation.

2.3. Modelling approach

In this study, a three-dimensional numerical model of the experimental setup was created to study the effect of EIE. The simulation domain included the soil portion of the experimental setup of dimension $1\ \text{m} \times 1\ \text{m} \times 0.8\ \text{m}$ with constant head boundary conditions on either side of the domain. The numerical model included a five-well system as shown in Figure 4. The injection extraction wells were placed at 35 cm c/c. For accurate three-dimensional analysis, the model was discretised into 100 rows, 100 columns, and 80 layers such that discretisation in all three dimensions remains the same ($\Delta x = \Delta y = \Delta z =$ 0.01 m). Three sets of simulations were conducted. One for passive spreading and the other for active spreading. In a passive simulation (which will be designated as case 1 from now on), the behaviour of the tracer injected at the central injection well in the absence of EIE was studied. The simulation was run for 195 min in three stress periods including observation taken till the end of the simulation. Active simulations were done for fully screened wells and partially screened wells which will be designated as case 2 and case 3 simulations, respectively, in subsequent discussions. Active simulations were also run for

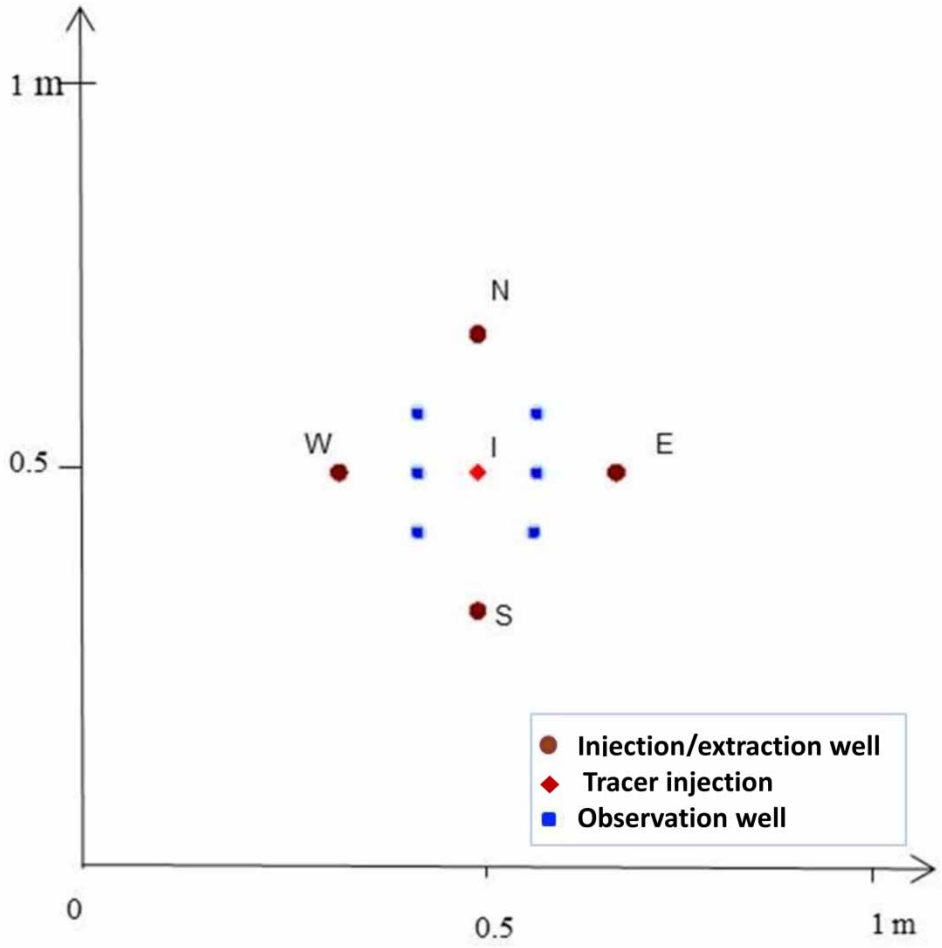

Figure 4 | Numerical model configuration.

195 min in 13 stress periods. Case 1 includes the tracer injection well (denoted by I in Figure 4) at the centre of the domain. Case 2 and case 3 include a central injection well along with four injection extraction wells at four sides (denoted by N,S,W and E in Figure 4). The screen depth details for case 2 and case 3 are illustrated using three-dimensional profile of the simulation domain as shown in Appendix (Supplementary material, Figure A3). The active screen depth for the north and west wells was kept at the top 0.37 m depth, and that for the south and east wells was kept at the bottom 0.37 m depth.

2.3.1. Numerical model description

The governing equation for transient groundwater flow with external source and sink is:

$$S_y \frac{\partial h}{\partial t} = \frac{\partial}{\partial x}\left(K_x h \frac{\partial h}{\partial x}\right) + \frac{\partial}{\partial y}\left(K_y h \frac{\partial h}{\partial y}\right) + \frac{\partial}{\partial z}\left(K_z h \frac{\partial h}{\partial z}\right) + \sum_{j=1}^{n} Q_j(t)\delta(X - X_j) \quad (3)$$

where K_x, K_y, and K_z are the hydraulic conductivity in x, y and z direction (L/T), S_y is storage property (specific yield), h is the head of groundwater, 'n' is the number of wells, Q_j is the injection rate in an active well, X is spatial coordinate (x, y, z), X_i is the position of well j and 'δ' is the Dirac delta function (Wang & Anderson 1995).

The governing equation for the spreading of a solute is given by the advection-dispersion equation. The advection-dispersion equation in three dimensions for a conservative solute is given by:

$$\frac{\partial C}{\partial t} = \frac{\partial}{\partial x}\left(D_x \frac{\partial C}{\partial x}\right) + \frac{\partial}{\partial y}\left(D_y \frac{\partial C}{\partial y}\right) + \frac{\partial}{\partial z}\left(D_z \frac{\partial C}{\partial z}\right) - \frac{\partial}{\partial x}(v_x\, C) + \frac{\partial}{\partial y}(v_y\, C) + \frac{\partial}{\partial z}(v_z\, C) \tag{4}$$

where D_x, D_y, and D_z represent dispersion coefficients (Equation (1)) in X, Y, and Z directions. C is the concentration of the solute. v_x,v_y, and v_z is the average linear velocity of groundwater in respective directions, and t is the time. The dispersion tensor for numerical mass transport simulation is obtained from (i) the longitudinal dispersivity of each transport grid cell (α_l), (ii) the ratio of horizontal (transverse) to longitudinal dispersivity (α_h/α_l), (iii) the ratio of vertical to longitudinal dispersivity (α_v/α_l) and (iv) molecular diffusion coefficient (D*) for each layer. Equation (2) shows the relationship between dispersion coefficient, dispersivity and molecular diffusion coefficient. The effect of molecular diffusion is negligible in this study and hence assumed as zero. The model parameters used in the numerical simulations are shown in Table 1.

2.3.2. Boundary conditions

Constant head boundary conditions with a head value of 0.8 m were provided on the eastern and western boundary of the model while no-flow boundary conditions were given for north and south boundaries. In the current study, head-dependent groundwater flow (initial groundwater flow) was kept at zero by providing equal heads on either side of the model. This helps in understanding the effect of advective transport created by using EIE alone. The initial head was also given as 0.8 m. Initial concentrations of 25 mg/l were assigned in all cells which was observed as the average concentration in observation wells prior to the experiment.

Pumping and extraction were incorporated into the model by using the pumping well boundary condition. Negative values of the pumping rate were used for extraction wells. A 12-step pumping schedule as shown in Figure 3, similar to that used in Asha *et al.* (2021) was used in this study. The pumping and extraction values were calculated based on non-dimensional numbers reported by Mays & Neupauer (2012) and then scaled down to a suitable value according to the size of the aquifer model and also to maintain a value less than the maximum pumping capacity of the syringe pump (viz. 100 ml/min). The pumping schedule is depicted in Figure 3 to have a better understanding and the positions of these wells are given in Figure 4.

The numerical simulation was conducted by using Visual MODFLOW Flex (version 7.1) which is a groundwater modelling software (Zheng & Wang 1999; Harbaugh *et al.* 2000). The numerical engines used to solve Equations (3) and (4) were MODFLOW (2005) and MT3DMS, respectively. For three-dimensional investigation, the model has been vertically discretized into 80 layers thereby keeping vertical discretisation equal to horizontal discretisation. The model was simulated in a transient state for 195 min divided into suitable stress periods for passive and active simulations.

Table 1 | Simulation parameters

Parameter	Values
Porous media thickness, b	0.8 m
Length and width of porous media	1 m × 1 m
Horizontal Discretisation (Δx, Δy)	0.01 m
Vertical Discretisation (Δz)	0.01 m
Duration of injection or extraction step, T	15 min
Porosity	0.36
Bulk density	1,740 kg/m^3
Horizontal hydraulic conductivity, $Kx = Ky$	0.000035 m/s
Vertical hydraulic conductivity, Kz (Todd & Mays 1989)	0.0000035 m/s
Longitudinal dispersivity (α_l) (experiment)	0.115 m
Ratio: α_h/α_l (calibrated)	0.2
Ratio: α_v/α_l (calibrated)	0.09

3. RESULTS AND DISCUSSIONS

An experimental investigation of EIE was conducted in this study by using a laboratory-scale tank model. Three sets of experiments and corresponding numerical simulations were carried out namely case: 1 (Passive simulation), case: 2 (active simulation with fully screened wells) and case 3(active simulation with partially screened wells). Numerical transport modelling was carried out in Visual MODFLOW flex by using the engine Modflow-2005 and MT3DMS. The experimental observations, calibration charts and numerical model results are explained in this section.

3.1. Experimental results

This study includes three sets of experiments – one passive set of experiments (case 1) and two active sets (case 2 and case 3) of experiments. The position of observation wells for all cases is shown in (Supplementary material, Figure A3).

A time series comparison of concentration among case 2 and case 3 experiments is presented in this section. Observations for active experiments were taken at three levels as indicated in Supplementary material, Figure A3. Figure 5 shows the observed concentration for case 2 and case 3 experiments at the mid-observation point of four selected observation wells (A2, A3, A4, A6). The results show that the rate of decrease of concentration is higher in case 3 (partially screened) than in case 2. In Figure 5, it can be seen that during the initial time steps, the difference in concentration between the two simulations remains low. The difference in concentration increases as the time step increases. This shows that a higher rate of

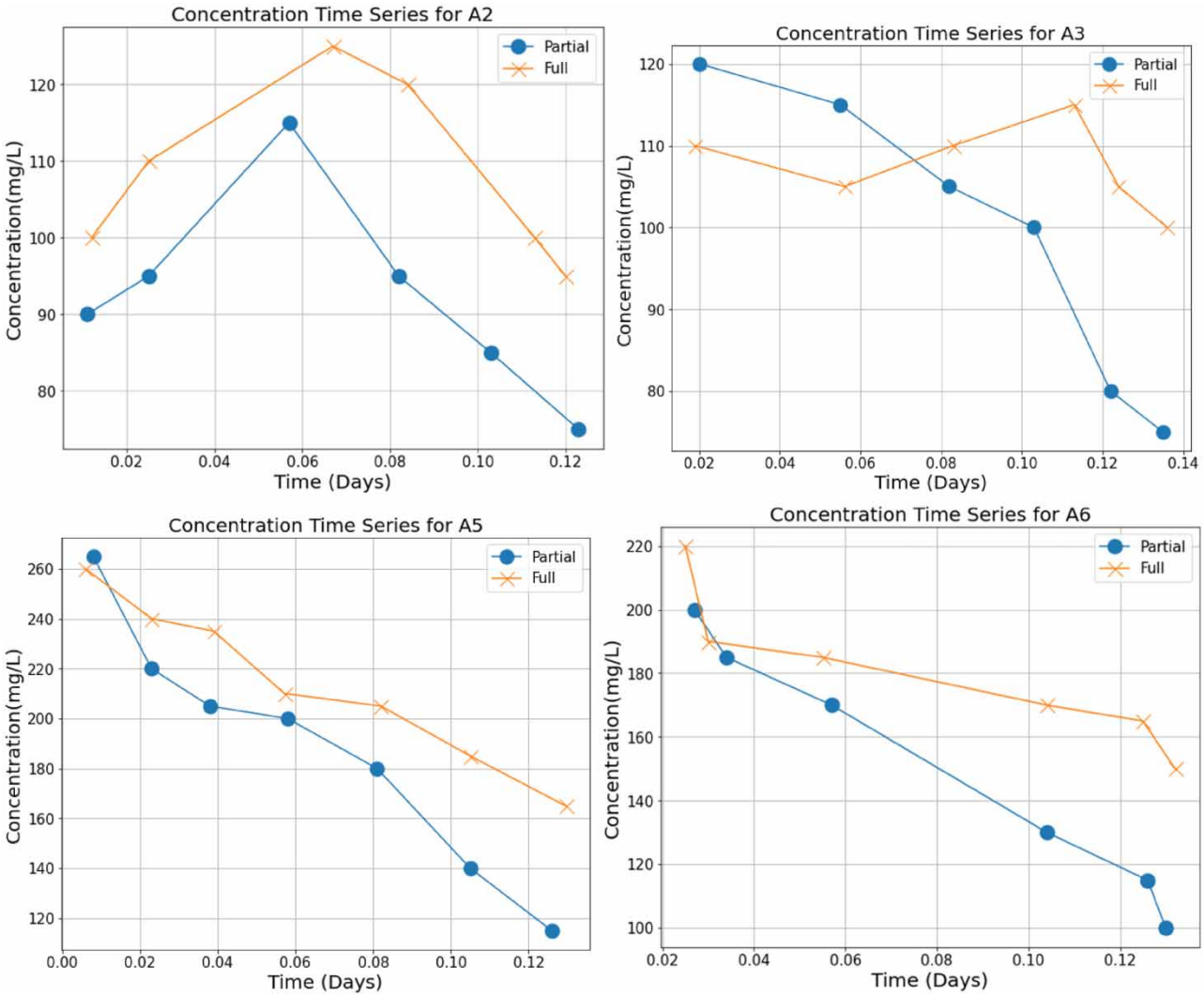

Figure 5 | Observed concentration time series (clockwise from left: well A2, A3, A6, and A5).

dilution takes place when EIE is carried out with partially screened wells. This difference is due to the fact that three-dimensional flow fields created as a result of partially screened wells dilute the plume at a faster rate as compared to fully screened wells.

It can also be seen that the final concentration at the end of the experiment in all wells lies at a lower level in case 3 than that in case 2. This concentration reduction indicates that EIE is more effective when flow fields are forced in vertical dimension by means of partially screened wells. It is to be noted that the difference in concentration reported in this section is just a representative value. The actual difference that is expected in the field is a multitude of this value, owing to the scale of the experiment. Hence, even a small difference or improvement observed in this experimental study is indicative of the large difference that could occur in the field.

3.2. Calibration and validation

It is essential to calibrate any numerical model either by experimental data or field data. The present study uses an experimental-scale model for this purpose. Almost all the parameters that are required for a numerical model were either measured or selected from the literature. The longitudinal dispersivity was kept at 0.115 m as obtained from the column experiment. The dispersivity ratios were calibrated by trial and error considering the observed concentration obtained during the experiment. During passive simulation, observations were taken from two layers closer to the injection layer. Spreading is much lower in the passive case, especially in the vertical direction and hence the ratio of horizontal to longitudinal dispersivity was calibrated by using this experiment. The vertical-to-longitudinal dispersivity ratio was calibrated using the observations taken at three layers in the active set of experiments. Final adjustments in ratios were carried out through trial and error such that a maximum correlation between numerical and experimental results was obtained. Horizontal to longitudinal dispersivity and vertical to longitudinal dispersivity ratio were calibrated as 0.2 and 0.09, respectively. The numerical results matched with experimental observations (omitting the outliers). Hence the model was calibrated and the calibrated value of dispersivity was used for the third set of simulations which showed a reasonable match with observed values. Thus the model was validated. The calibration charts are shown in Supplementary material, Figure A4–A6 and details of error analysis are tabulated in Table 2.

The correlation coefficient of greater than 0.98 and normalised RMS error of less than 10% were obtained for all three cases (Table 2). From the correlation coefficients, standard error estimate, RMS and normalised RMS, it is evident that the simulated results and experimental results match with reasonable accuracy. An exact match between simulated and observed results was not obtained owing to the fact that the numerical model is based on the assumption of homogeneity of porous media which is not the case with the experiment. Even though the soil has been filled carefully to ensure a uniform distribution of properties, 100% homogeneity cannot be expected.

3.3. Concentration contours

The contours resulting from the injected tracer solution showed varying plume dynamics under various scenarios of pumping. The three cases discussed here are passive spreading without EIE (case 1); Active spreading with fully screened wells in EIE (case 2); and active spreading with partially screened wells in EIE (case 3). Figure 6(a)–6(c) shows the three-dimensional view of the tracer plume at the end of the simulation for the three cases.

The three-dimensional view of concentration contours at the end of the simulation indicates that spreading and dilution increase when EIE is introduced. The initial concentration injected was 1,500 mg/l of conservative tracer. It was observed

Table 2 | Error analysis

Case	Correlation coefficient	Root-mean squared (mg/L)	Normalised RMS(%)
1	0.98	6.69	5.35
2	0.99	7.97	3.32
3	0.99	7.96	3.32

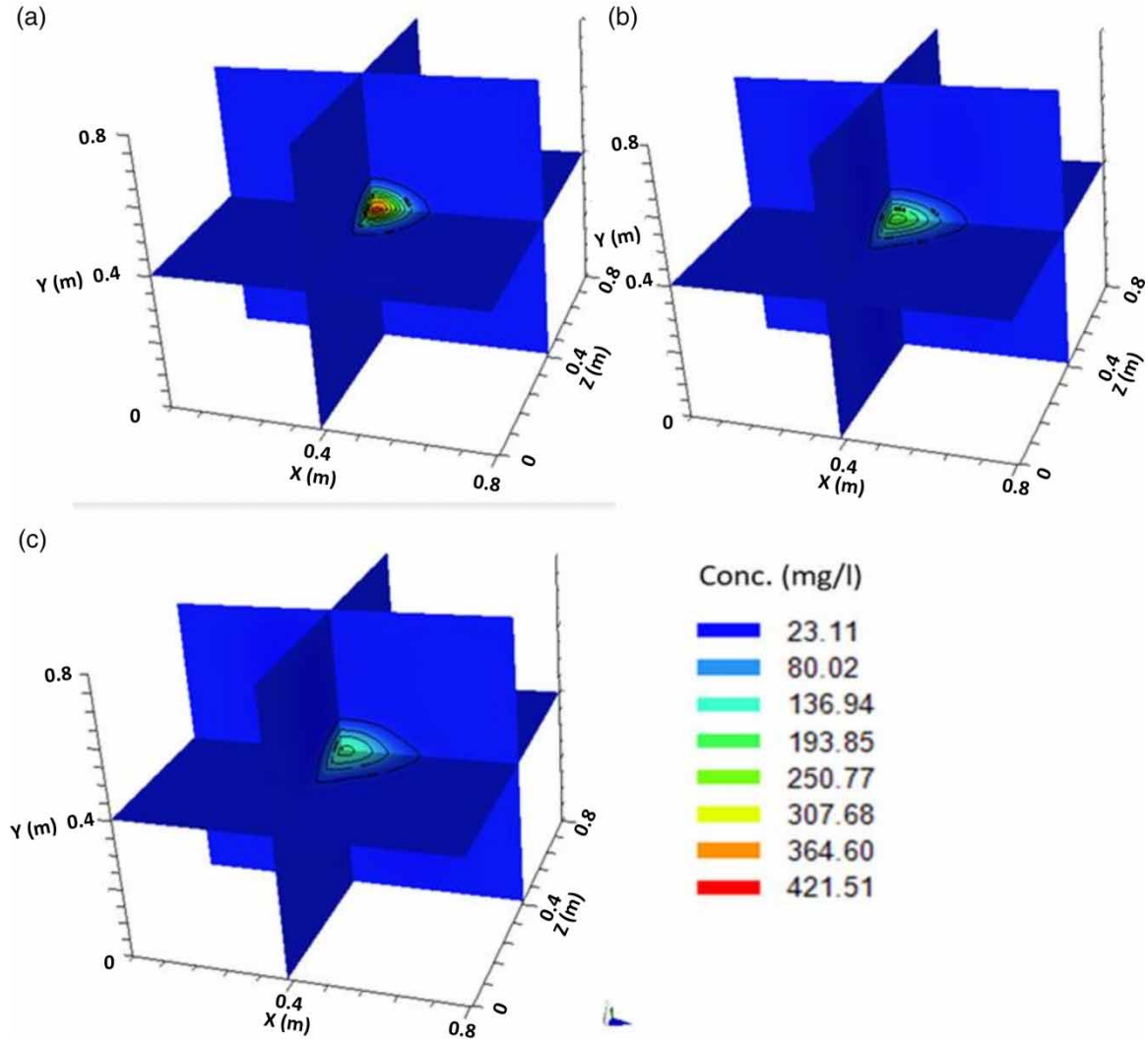

Figure 6 | 3-D view of concentration contour at the end of simulation (a: case 1; b: case 2; c: case 3).

that the maximum concentration decreased to approximately 419.29 mg/l in case 1 while that in case 2 to 211.73 mg/l and in case 3, to 163.58 mg/l. In case 1, the advective transport occurs during the tracer injection period (initial 15 min) and continues until the head created due to injection reduces to the initial head. The dilution occurs as a result of dispersion, anisotropy and advection caused by the injection head. The dilution because of dispersion and anisotropy continues even after the advection stops (as in case 1). In case 2, the spreading occurs mainly due to advective transport created by active EIE protocol along with dispersion and anisotropy. The advective transport causes more spreading and dilution of the plume compared to case 1. In case 3, advective transport in the vertical direction also takes place in addition to the spreading happening in case 2. The advective transport in the vertical direction further increases the spreading across layers and dilutes the plume. Hence, maximum dilution and more spread are observed in the case 3 where three-dimensional flow was induced by using partially screened wells.

The higher reduction in concentration observed in case 3 is an added advantage in the case of remediation processes because the enhanced reduction in concentration results from enhanced elongation of the plume. To have a better insight into the processes of spreading the concentration contours obtained in the mid layer (X–Y plane; layer view), mid row (X–Z plane: row view) and mid column (Y–Z plane: column view) for two different times are shown in Figure 7(a) and 7(b). The plume dynamics for all three cases at 75 and 195 min are shown in Figure 7(a) and (b), respectively.

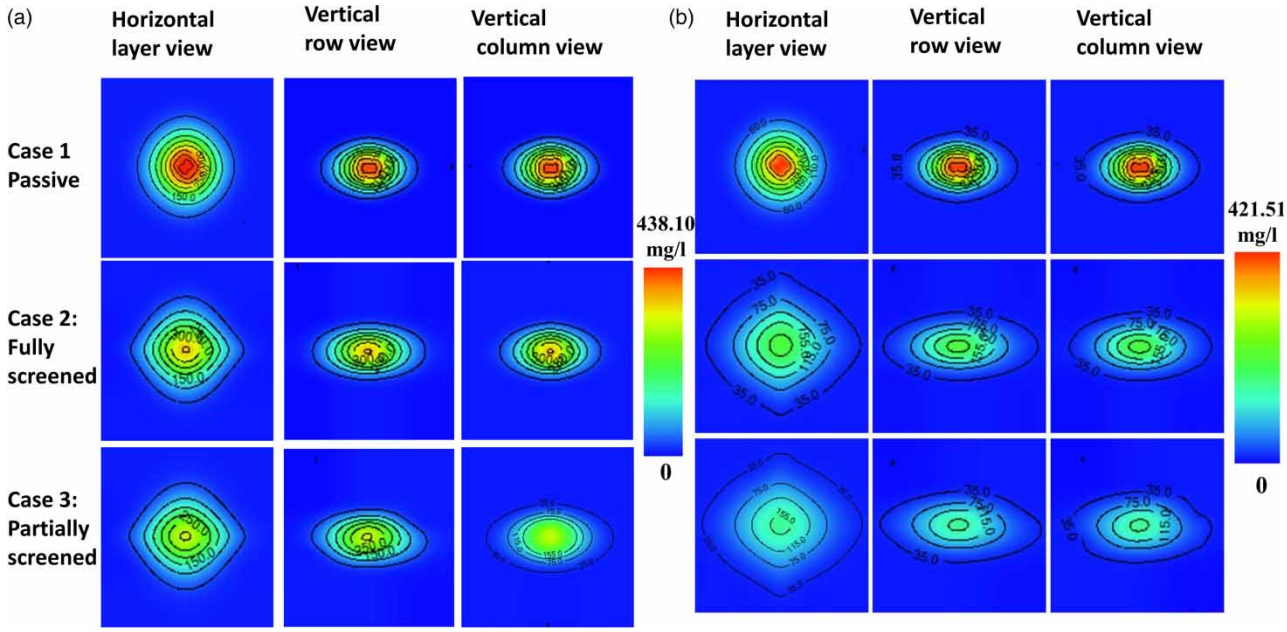

Figure 7 | (a) Horizontal and vertical views along layer, row and columnof three cases at 75 min. (b) Horizontal and vertical views along layer, row and column of three cases at 195 min.

At initial stress periods, the concentration contours show the pattern of a concentric circle in the horizontal view with maximum concentration at the injection point and an oval shape in the vertical view for all the cases. Major distinctions in plume dynamics cannot be made at this stage. At 75 min, there is no peculiar deviation from the circular dispersion of contour in case 1. This is because of the passive spreading nature, where the spreading takes place by virtue of dispersion and advection in response to the head created by injection; while in case 2 and case case 3 the shape of the contour shows a diamond shape in layer view (Figure 7(a) and 7(b)). More dilution is observed in case 3 than in case 2. In case 3, the elongation of contours also takes place diagonally owing to vertical flow in response to partially screened wells. Plume distortion is found in case 3 which is more evident in row view at 75 min (Figure 7(a)). This is due to the flow field created by diagonally opposite partially screened wells of an east-west pair of wells (at 75 min) and is evidence of enhanced plume extension in the vertical plane. Hence more dilution is observed in case 3. Similarly, the partially screened north–south wells tend to create plume distortion which can be seen in column view at 195 min (Figure 7(b)). These plume distortions in the vertical direction are the reason behind more dilution in case 3.

3.4. Quantification of results

The results of numerical simulations were quantified in terms of solute mass attenuation. A fixed concentration of tracer solution was injected at the centre of the domain for all the cases of simulation. The degree of solute mass reduced was calculated for each case as follows. The solute mass attenuation M (%) is given by:

$$M = \frac{M_i - M_f}{M_i} \times 100 \tag{5}$$

where M_i is the initial concentration of tracer solute injected into the domain (1,500 mg/l), M_f is the final maximum concentration at the end of simulation for each case. The final concentration in case 1, case 2 and case 3 were observed as 419.29, 211.96, and 163.58, respectively. It can be seen that a prominent differentiation can be made by comparing the percentage of solute mass attenuated at the end of the simulation for the three cases. The value of 'M' was obtained as 72.04, 85.86, and

89.09% for case 1, case 2, and case 3, respectively. A considerable decrease was observed in final concentration at the point of introduction for case 3 which showed a reduction of almost 90% from initial concentration. This shows fairly good improvement of spreading in case 3. This was also observed experimentally (the final concentration of observation wells was found lower in case 3 (in Figure 7)) hence showing the role of partially screened wells in enhancing plume dilution.

4. CONCLUSIONS

The practical difficulty in conducting experimental studies in EIE is high. In this context, a three-dimensional experimental simulation of tracer spreading in response to EIE is a step towards further improvement in this technology. This paper illustrates the effect of EIE on the transport of a conservative tracer in real porous media by using a three-dimensional experimental setup. The purpose of the experiment was to validate and improve numerical simulations of EIE available in the literature, particularly the effect of partially screened wells as reported by Asha *et al.* (2021). Screen depth variation and its effectiveness have been carefully formulated in this study and a comprehensive conclusion has been derived.

- Enhancement in the transport of tracer solution is observed when EIE is made in three dimensions by replacing the screen depth appropriately forcing the flow in three dimensions. This was proved both experimentally and numerically by properly validating the model with experimental data. With active screen depth emplaced at different vertical levels, the contours elongated diagonally causing plume stretching and dilution.
- The time series observation from the experiment indicates that case 3 (EIE with partially screened wells) shows consistently lower concentration when compared to case 2 (EIE with fully screened wells). This shows that partially screened wells work better than fully screened wells in diluting the plume keeping all other conditions the same. Here dilution can be attributed to the higher rate of dispersion of the plume, which indirectly shows that partially screened wells enhance the plume area available for reaction. Concentrations at observation wells show higher dilution in case 3 thus reinforcing the finding that partially screened wells give higher dilution within real porous media. During an in situ porous media treatment, the scenario mentioned above will increase the rate of reaction. Hence, just an emplacement can lead to better solute transport without any increase in the cost of treatment.
- The spread quantified in terms of solute mass attenuation also shows maximum spreading for case 3, which matches with the experimental results.
- The model validated in this study can be easily reproduced for further numerical simulations including flow-through models, continuous injection models or any complex models related to active spreading. The model can also be adapted for optimisation of different elements of EIE to maximise spreading in three dimensions which will render guidance to field application of EIE.
- The experimental setup can be further used for analysing the effect of EIE in under flow-through conditions and different patterns of pumping. It can also be reused for different types of soil and layered soil study.

DATA AVAILABILITY STATEMENT

All relevant data are included in the paper or its Supplementary Information.

CONFLICT OF INTEREST

The authors declare there is no conflict.

REFERENCES

Asha, F. M., Sajikumar, N. & Subaida, E. A. 2021 Three-dimensional investigation of engineered injection and extraction for enhanced groundwater remediation. *Journal of Hydrologic Engineering (ASCE)* **26** (8). 04021028-1-12. https://doi.org/10.1061/(ASCE)HE.1943-5584.0002114.

Bagtzoglou, A. C. & Oates, P. M. 2007 Chaotic advection and enhanced groundwater remediation. *Journal of Materials in Civil Engineering* **19** (1), 75–83.

Bear, J. 1972 *Dynamics of Fluid in Porous Media*. Elsevier, New York, NY, USA.

Cho, M. S., Solano, F., Thomson, N. R., Trefry, M. G., Lester, D. R. & Metcalfe, G. 2019 Field trials of chaotic advection to enhance reagent delivery. *Ground Water Monitoring & Remediation* **39** (3), 23–39. https://doi.org/10.1111/gwmr.12339.

Freeze, R. A. & Cherry, J. A. 1979 *Groundwater*. Prentice-Hall, United Kingdom.

Greene, J. A., Neupauer, R. M., Ye, M. & Kasprzyk, J. R. 2017 Engineered injection and extraction for remediation of uranium-contaminated groundwater. In: *Proc., World Environmental and Water Resources Congress 2017*, Reston, VA. ASCE, pp. 111–117.

Harbaugh, A. W., Banta, E. R., Hill, M. C., Mcdonald, M. G. & Groat, C. G. 2000 MODFLOW-2000, The U.S. Geological Survey Modular groundwater Model User Guide to Modularization Concepts and the Groundwater Flow Process. U.S. Geological Survey, Open-File Report 00-92, U.S. Department of the Interior.

Huang, K., van Genuchten, M. T. & Zhang, R. 1996 Exact solutions for one-dimensional transport with asymptotic scale-dependent dispersion. *Applied Mathematical Modelling* **20**, 298–308.

Jones, S. W. & Aref, H. 1988 Chaotic advection in pulsed source-sink systems. *Physics of Fluids* **31** (3), 469–485. https://doi.org/10.1063/1.866828.

Kapoor, V. & Kitanidis, P. K. 1996 Concentration fluctuations and dilution in two-dimensionally periodic heterogeneous porous media. *Transport in Porous Media* **22** (1), 91–119. https://doi.org/10.1007/BF00974313.

Li, L., Steefel, C. I., Williams, K. H., Wilkins, M. J. & Hubbard, S. S. 2009 Mineral transformation and biomass accumulation associated with uranium bioremediation at Rifle, Colorado. *Environmental Science & Technology* **43** (14), 5429–5435. https://doi.org/10.1021/es900016v.

Matko, V. 2003 Porosity determination by using stochastics method. *Sensors and Actuators A* **44** (3–4), 155–162.

Mays, D. C. & Neupauer, R. M. 2010 Engineered well injection and extraction to enhance mixing in aquifers. In: *Proc., World Environmental and Water Resources Congress 2010: Challenges of Change*, Reston, VA. ASCE, pp. 715–722.

Mays, D. C. & Neupauer, R. M. 2012 Plume spreading in groundwater by stretching and folding. *Water Resources Research* **48** (7), 1–10. https://doi.org/10.1029/2011WR011567.

Neupauer, R. M. & Mays, D. C. 2015 Engineered injection and extraction for in situ remediation of sorbing solutes in groundwater. *Journal of Environmental Engineering (United States)* **141** (6), 04014095. doi: 10.1061/(ASCE)EE.1943-7870.0000923.

Nissan, A., Dror, I. & Berkowitz, B. 2017 Time-dependent velocity field controls on anomalous chemical transport in porous media. *Water Resources Research* **53**, 3760–3769. https://doi.org/10.1002/2016WR020143.

Ogata, A. 1970 Theory of dispersion in granular media. *US Geol. Sur. Prof. Paper* **411**, 1–34.

Ottino, J. 1990 Mixing, chaotic advection, and turbulence. *Annual Review of Fluid Mechanics* **22** (1), 207–253. doi:10.1146/annurev.fluid.22.1.207.

Piscopo, A. N., Neupauer, R. M. & Mays, D. C. 2011 Contrasting advective spreading and dispersive mixing. In *World Environmental and Water Resources Congress 2011: Bearing Knowledge for Sustainability – Proceedings of the 2011 World Environmental and Water Resources Congress*. doi: 10.1061/41173(414)98.

Piscopo, A. N., Neupauer, R. M. & Mays, D. C. 2013 Engineered injection and extraction to enhance reaction for improved in situ remediation. *Water Resources Research* **49** (6), 3618–3625. doi: 10.1002/wrcr.20209.

Piscopo, A. N., Kasprzyk, J. R. & Neupauer, R. M. 2015 An iterative approach to multi-objective engineering design: Optimization of engineered injection and extraction for enhanced groundwater remediation. *Environmental Modelling and Software, Elsevier Ltd* **69**, 253–261. doi: 10.1016/j.envsoft.2014.08.030.

Radabaugh, C. R., Mays, D. C. & Neupauer, R. M. 2009 Groundwater mixing using pulsed dipole injection/extraction wells. In *Proc., World Environmental and Water Resources Congress 2009: Great Rivers*, Reston, VA. ASCE.

Raghunath, H. M. 2007 Groundwater Chapter: 10.1.3. New Age International.

Roth, E. J. 2018 Experimental investigation of scalar spreading by engineered injection and extraction in porous media. *Civil Engineering graduate theses and dissertations*, Dept. of Civil Engineering, Univ. of Colorado.

Sposito, G. 2006 Chaotic solute advection by unsteady groundwater flow. *Water Resources Research* **42** (6), 1–6. https://doi.org/10.1029/2005WR004518.

Stremler, M. A., Haselton, F. R. & Aref, H. 2004 Designing for chaos: Applications of chaotic advection at the microscale. *Philosophical Transactions of the Royal Society A: Mathematical, Physical and Engineering Sciences* **362** (1818), 1019–1036. doi:10.1098/rsta.2003.1360.

Todd, D. K. & Mays, L. W. 1989 *Groundwater Hydrology Chapter:3*. Wiley, Hoboken, NJ, US.

Trefry, M. G., Lester, D. R., Metcalfe, G., Ord, A. & Regenauer-Lieb, K. 2012 Toward enhanced subsurface intervention methods using chaotic advection. *Journal of Contaminant Hydrology* **127** (1–4), 15–29. https://doi.org/10.1016/j.jconhyd.2011.04.006.

Wang, H. F. & Anderson, M. P. 1995 *Introduction to Groundwater Modeling: Finite Difference and Finite Element Methods*. Academic Press, London, UK.

Zhang, P., DeVries, S. L., Dathe, A. & Bagtzoglou, A. C. 2009 Enhanced mixing and plume containment in porous media under time-dependent oscillatory flow. *Environmental Science and Technology* **43** (16), 6283–6288. https://doi.org/10.1021/es900854r.

Zheng, C. & Wang, P. P. 1999 MT3DMS: A modular three-dimensional multispecies model for simulation of advection, dispersion, and chemical reactions of contaminants in groundwater systems. Documentation and user's guide. Contract report SERDP-99-1. U.S. Army Engineer Research and Development Center, Vicksburg, MS.

Zhuang, L., Raoof, A., Mahmoodlu, M. G., Biekart, S., de Witte, R., Badi, L., van Genuchten, M. T. & Lin, K. 2021 Unsaturated flow effects on solute transport in porous media. *Journal of Hydrology* **598**, 126301.

First received 24 September 2023; accepted in revised form 29 November 2023. Available online 15 December 2023